Heliopause imaging in EUV: Oxygen O+ ion 83.4-nm resonance line emission

Mike Gruntman

Department of Aerospace Engineering, University of Southern California, Los Angeles

Hans J. Fahr

Institut für Astrophysik und Extraterrestrische Forschung, Universität Bonn, Bonn, Germany

Abstract. We explore the possibility of remote, from 1 AU, study of the heliopause by an observer outside the geocorona. We argue that the heliopause, a boundary that separates the solar wind and the galactic plasma of the local interstellar medium (LISM), can be imaged by detecting solar extreme ultraviolet (EUV) radiation reflected by interstellar ions. Such EUV imaging would map the heliopause and provide important insight into its three-dimensional structure and the LISM parameters as well. We consider heliopause mapping in the oxygen O+ ion resonance line (83.4 nm); imaging in the helium He+ ion line (30.4 nm) will be considered in a future article. We show that the expected heliopause brightness map at 83.4 nm is essentially different from that of the foreground glow of the solar wind O+ pickup ions. The interstellar plasma glow is brighter in the upwind (with respect to the interstellar wind) direction, while the pickup ion glow dominates in the downwind direction. The spectral characteristics of the radiation scattered by the LISM plasma and by the pickup ions are significantly different. The all-sky images at 83.4 nm are highly sensitive to the ionization state of the LISM and would allow one to probe the asymmetry of the interstellar magnetic field. We briefly discuss the experimental requirements to heliopause EUV mapping, which would require 3 orders of magnitude improvement in instrumentation sensitivity. This is a challenging but not impossible task.

1. Introduction

The interaction of our star, the Sun, with the surrounding interstellar medium leads to the buildup of the heliosphere, that is the region where the Sun controls the state and behavior of the plasma environment [*Davis*, 1955; *Parker*, 1961; *Dessler*, 1967; *Axford*, 1972, 1990; *Fahr and Fichtner*, 1991]. The heliosphere is a complicated phenomenon where solar wind and interstellar plasmas, neutral interstellar gas, magnetic field, and anomalous and galactic cosmic rays play prominent dynamic roles (Figure 1). The heliosphere is an example of a commonplace, as confirmed by the recent observations of *Wood and Linsky* [1998], but fundamental astrophysical phenomenon, the formation of an astrosphere.

The heliosphere was extensively studied both theoretically and by various experimental techniques since the early 1960s. Significant progress was achieved in understanding interaction between the Sun and the local interstellar medium (LISM), but many important questions are yet unanswered, for example: Is the solar wind expansion terminated by a shock? What is the nature of the shock? What is the distance to and shape of the heliopause, a boundary that separates the solar wind plasma and the galactic plasma of the LISM? Is the heliopause stable? What is the ionization state of interstellar gas in the LISM? What is

the direction and magnitude of the interstellar magnetic field? Is the interstellar wind subsonic or supersonic? Is a bow shock formed in front of the heliosphere?

Experimental data on the heliospheric interface region are exceptionally scarce, mostly indirect, and often ambiguous. A self-consistent model of the stationary heliosphere has yet to be built, and some aspects of the interaction, for example, temporal variations (heliosphere "breathing"), instabilities, and processes in the heliospheric tail are not satisfactorily understood, not even on a qualitative level. Furthermore, the physics and state of the LISM [*Cox and Reynolds*, 1987; *Frisch*, 1990, 1995; *Reynolds*, 1990; *Dupuis et al.*, 1995; *Breitschwerdt*, 1996] are not known in many important details.

It is believed that in several years, Voyager 1 will plunge into the solar wind termination shock (Figure 1) that converts the supersonic solar wind flow into a subsonic one. The spacecraft, now at ~75 AU, will thus establish the distance to the termination shock in one direction. Voyager 1 is headed toward approximately the upwind direction (with respect to the interstellar wind), and the termination shock is estimated to be somewhere between 80 and 100 AU.

We know very little about the heliopause with the direct experimental data next to nonexistent [*Suess*, 1990]. The heliopause separates interstellar and solar wind plasmas with the number densities 2 orders of magnitude different. We do not know whether a stable boundary exists in such conditions. The only measurements that may be directly related to the heliopause are thought to be those of the 2-3 kHz radio emissions detected by Voyager [*Gurnett and Kurth*, 1996].
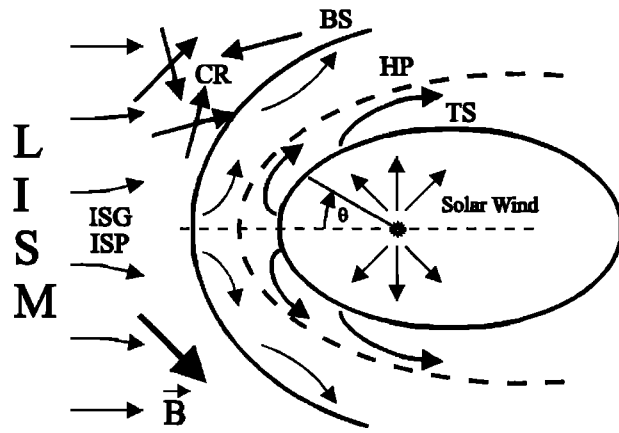
Figure 1. Possible solar wind interaction (two-shock model) with the local interstellar medium (LISM). TS, termination shock; HP, heliopause; BS, bow shock; CR, cosmic rays; ISP(G), interstellar plasma (gas); B, magnetic field. Angle θ is counted from the upwind direction.

Although Voyagers are anticipated to provide first in situ measurements of some important parameters of the postshock solar wind plasma, the spacecraft may still be 50-100 AU away from the heliopause. Voyagers may not reach the heliopause by the projected end of their lifetimes (~2025). Moreover, the spacecraft were designed for planetary flybys and were not optimally instrumented for study of the heliospheric interface region. The planned (and optimally instrumented) Interstellar Probe mission would cross the termination shock, reach the heliopause, and in situ explore LISM in one direction some time after 2020 [*Liewer et al.*, 2000].

The heliosphere is essentially an asymmetric, three-dimensional (3-D) object because 1) partially ionized interstellar gas of the LISM moves with a 26-km s⁻¹ speed [*Lallement et al.*, 1993; *Witte et al.*, 1996] with respect to the Sun (interstellar wind); 2) solar wind is significantly anisotropic [e.g., *McComas et al.*, 1998]; and 3) the interstellar magnetic field can be pointed in any direction with respect to the interstellar wind velocity vector. The heliosphere asymmetry and its size call for remote experimental techniques to study the heliospheric boundary. Only remote observations, preferably not far from 1 AU, can provide a global view of the 3-D heliosphere on a continuous basis. Voyager 1 would complement such remote imaging by "ground truth," in situ measurements in one direction.

Is there a way to obtain remotely the experimental data that would significantly advance our understanding of the solar system interaction with the LISM and properties of the heliospheric boundary? It was argued for some time that the processes at the termination shock and in the heliosheath (the region between the termination shock and heliopause) can be remotely studied by measuring the fluxes of energetic neutral atoms (ENAs) produced by the postshock compressed and heated solar wind plasma and pickup protons [*Gruntman*, 1992a, 1997; *Hsieh and Gruntman*, 1993; *Gruntman et al.*, 1999; M. Gruntman et al., ENA imaging of the heliospheric boundary region, manuscript in preparation, 2000]. Global heliosphere images in the 0.2–10 keV ENA fluxes are most promising to probe the structure and nature of the termination

shock and evolution of the pickup protons at and beyond the shock (Gruntman et al., manuscript in preparation, 2000). *Hilchenbach et al.* [1998] recently reported the first probable detection of the heliospheric ENAs in a much higher energy (55-80 keV) range.

The heliosphere is a complex object. Understanding it requires establishing a three-dimensional global structure of both the termination shock and the heliopause and accurate knowledge of the LISM parameters. ENA imaging and Voyagers would allow us to explore the termination shock and the postshock solar wind plasma in the heliosheath. Is there a way to take the next step and map the heliopause and probe the LISM plasma flow beyond it remotely?

We argue that the heliopause can be explored remotely, from 1 AU [*Gruntman and Fahr*, 1998]. The LISM plasma beyond the heliopause is much denser, ~2 orders of magnitude, than the solar wind plasma in the heliosheath. Interstellar singly charged ions like He⁺, O⁺, Ne⁺, etc. would resonantly scatter the corresponding solar EUV-line emissions as a special signature. Measurements of the solar extreme ultraviolet (EUV) radiation reflected from the interstellar plasmas flowing around the heliopause would open access to the heliopause and the region beyond. Heliopause imaging would map the heliopause and provide an important insight into the LISM ionization state and asymmetry of the interstellar magnetic field.

In this article we consider the expected LISM plasma oxygen O⁺ ion glow at 83.4 nm and evaluate the background and foreground radiation in this spectral range. Possible heliopause imaging in the helium He⁺ ion 30.4-nm line will be discussed in a future article. The first brief results of this study were published elsewhere [*Gruntman and Fahr*, 1998]. The geocoronal line emissions in EUV are much stronger than the expected heliospheric interface emissions at 83.4 nm [*Chakrabarti et al.*, 1982, 1984]. Therefore the heliopause EUV mapping can only be done from a spacecraft well outside the geocorona. Heliopause mapping would require 3 orders of magnitude improvement in the existing instrumentation. This is a challenging but not impossible task.

2. Heliopause Mapping in EUV

The Sun is a bright source of radiation that excites an atom (ion) when the solar photon wavelength corresponds to the atomic transition. Since most of interstellar and heliospheric atoms and ions are in the ground state, the transitions of interest are in the EUV spectral range. Solar radiation in EUV consists of a number of line emissions and continuum radiation. At the resonance transition of O⁺ (O II), 83.4 nm, the solar continuum radiation is attributed to H I continuum [*Warren et al.*, 1998].

An excited atom (ion) would return to the lower state with a spontaneous emission of a photon. This emission may occur in all directions, including the direction back toward the Sun, with the angular dependence of scattering described by the so-called phase function. Ions and atoms would thus "glow" under solar illumination. Glow measurements allow one to remotely study the properties of the radiation scattering particles. Global heliospheric populations of interstellar hydrogen and helium neutral atoms have been extensively studied by such a technique since the 1960s [e.g., *Fahr*, 1974; *Holzer*, 1977; *Thomas*, 1978; *Bertaux*, 1984].

Interstellar neutral atoms are not suitable for heliopause mapping because the atoms penetrate deep into the heliosphere.

Therefore most of the detectable glow observed near Earth's orbit would originate close to the Sun (< 20 AU). It is important that interstellar ions cannot cross the heliopause boundary and so flow around the heliopause. Hence the detection of the solar EUV emissions reflected from interstellar ions would allow one to probe LISM plasma properties beyond the heliopause boundary.

Feasibility of heliopause EUV mapping critically depends on the brightness of the solar line and its spectral profile, the interstellar ion abundance, and the other sources of radiation (background and foreground) in the spectral range of interest. Interstellar gas is partially ionized and has a temperature of 7000-8000 K in the LISM [Lallement et al., 1993; Witte et al., 1996]. Interstellar gas is not in thermodynamical equilibrium, and the ionization states of its various constituents are not accurately known. The gas consists of hydrogen (~90%), helium (~10%), and minor constituents. The ions of the most abundant interstellar gas component, the protons, cannot be imaged optically. Interstellar helium and oxygen ions are the most attractive candidates for heliopause mapping. We concentrate in this work on heliopause imaging in the oxygen O^+ ion resonance (83.4-nm) line.

Interstellar oxygen O^+ ions are ideally suited for heliopause mapping for the following reasons. First, oxygen is the most abundant species among the interstellar gas minor constituents. Second, background galactic radiation is minimal at 83.4 nm because the photoionization cross section of atomic hydrogen is close to maximum at this wavelength. Third, abundance of oxygen ions other than singly charged O^+ is negligible under the LISM conditions. Finally, the measurement of the ionization state of oxygen allows one to directly infer the ionization state of hydrogen, the most abundant constituent of the LISM. The ionization potential of atomic oxygen nearly matches the ionization potential of hydrogen atoms, which results in large hydrogen-oxygen charge exchange cross sections. The efficient charge exchange coupling between hydrogen and oxygen in partially ionized plasmas establishes a relation between their ionization states in the LISM, $\xi_O/\xi_H \approx 8/9$, where ξ_O and ξ_H are the fractional ionizations ($n_{ION}/n_{NEUTRAL}$) of oxygen and hydrogen, respectively [Field and Steigman, 1971].

Heliopause imaging at 83.4 nm opens a most promising way to establish the ionization state of interstellar oxygen (see Section 6) and, correspondingly, hydrogen. Interstellar hydrogen, the dominant constituent of LISM, is most important in determining the heliosphere size and shape. Other LISM constituents are of only secondary importance as contributors to the LISM pressure and plasma flow dynamics. The ionization state of helium, however, is important for understanding the physics of LISM, in particular the processes of ionization and recombination [Cox and Reynolds, 1987; Frisch, 1995; Dupuis et al., 1995; Frisch and Slavin, 1996].

The interstellar wind plasma flow carries O^+ ions that cannot cross the heliopause and have to move around its outer surface. One can imagine the Sun surrounded by a LISM O^+ ion "wall" beyond the "empty" cavity limited by the heliopause boundary. Individual O^+ ions would scatter solar radiation, with the scattering rates determined by their respective Doppler shifts from the line center and distances from the Sun. One can thus introduce an effective g factor for a given ion population, allowing for the local ion thermal motion and bulk velocity with respect to the sun. The effective g factor is defined as an average number of photons scattered per second per atom (ion)

for a given ion population. Figure 2 illustrates the photon-scattering geometry. The scattered photons that reach an observer looking in the antisolar direction are those with the scattering angle $\varphi = \pi$. In this work, we consider the two-dimensional (symmetric about the interstellar wind velocity vector) heliosphere; the problem can be readily extended to a more general three-dimensional case.

The g factor is often used to describe the scattering rate at 1 AU [e.g., Meier, 1991]. However, it is more convenient in this work to use the effective local scattering rate $g(R)$ that includes the solar radiation $\sim 1/R^2$ dependence. The scattering medium is essentially optically thin in our case, and $g(R) = g_E (R_E/R)^2$, where $g_E = g(R_E)$ is the effective scattering rate of a given ion distribution at $R_E = 1$ AU.

We consider only the photon fluxes as seen by an observer looking exactly in the antisolar direction. The following treatment can be applied in a straightforward manner to an arbitrary direction. A radiance of scattered photons (photon (cm^2 s sr)$^{-1}$), $F(\theta)$, reaching an observer at 1 AU for an isotropic scattering phase function is an integral along the line of sight

$$F(\theta) = \frac{1}{4\pi} \int_{R_E}^{\infty} N_{O+}(R,\theta)\, g(R,\theta)\, dR \ , \qquad (1)$$

where the g factor depends on the distance from the Sun and local velocity distribution function and $N_{O+}(R,\theta)$ is the local O^+ ion number density. Angle θ, describing the observation direction with respect to the LISM wind vector, is counted from the upwind direction (Figure 1).

For a simplified case of a vanishing O^+ ion number density inside the heliopause ($R < R_{HP}$) and interstellar plasma beyond the heliopause with a uniform O^+ number density $N_{O+,LISM}$, constant temperature and at rest, (1) would give

$$F(\theta) = \frac{1}{4\pi} N_{O+,LISM}\, g_E$$

$$\times \int_{R_{HP}}^{\infty} \left(\frac{R_E}{R}\right)^2 dR = \frac{N_{O+,LISM}\, g_E\, R_E^2}{4\pi} \frac{1}{R_{HP}(\theta)} \ . \qquad (2)$$

The sky brightness is inversely proportional to the distance R_{HP} to the heliopause in the direction of observation θ. Thus heliosphere imaging in the O II resonance line is a way to establish the distance to and shape of the heliopause. Certainly, the detailed temperature, velocity, and number density flow fields of the LISM plasma are needed for accurate treatment of the problem. The sensitivity of the interstellar ion glow to the
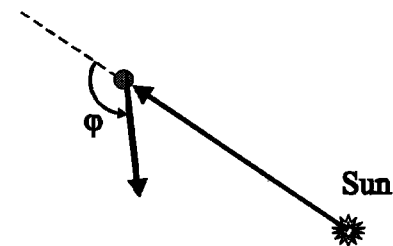

Figure 2. An incident solar photon is scattered by an angle φ. The g factor is defined as the number of photons scattered per second per ion; the g factor depends on the solar line profile, distance from the Sun, and the atom (ion) velocity.

plasma flow parameters and the shape of the heliopause makes EUV imaging a promising tool to study the heliospheric interface region.

3. Heliopause and Global Plasma Flow

The global flow field (velocity, temperature, number density) of the LISM and solar wind plasmas and the heliospheric interface structure were calculated for this work under an assumption of a two-shock model of the LISM interaction with the solar wind. (The calculations were performed by V. Baranov and his group at the Russian Academy of Sciences.) The two-shock model assumes that both the interstellar plasma and solar wind plasma flows are supersonic, the plasma-gas coupling is treated self-consistently, the neutral component is described kinetically, and cosmic rays and the interstellar magnetic field are disregarded [*Baranov and Malama*, 1993, 1995; *Baranov et al.*, 1998].

The following LISM parameters (at infinity) were used in our example: velocity, 25 km s^{-1}; temperature, 5672 K; electron (proton) number density, $n_e = 0.07$ cm^{-3}; neutral hydrogen number density, $n_H = 0.14$ cm^{-3}. The solar wind was assumed to flow spherically symmetric with a velocity of 450 km s^{-1} and a number density of 7 cm^{-3} at 1 AU. The calculated heliospheric interface surfaces are shown in Figure 3. The velocity, temperature, and number density of the interstellar plasma and solar wind plasma flows were calculated in the region from 400 AU in the upwind direction down to 700 AU in the heliospheric tail and 1400 AU in the side-wind direction.

LISM oxygen was assumed to be present everywhere beyond the heliopause in cosmic abundance, that is 7×10^{-4} by number of atoms relative to hydrogen. The accuracy of the neutral number density calculations in the Sun's immediate
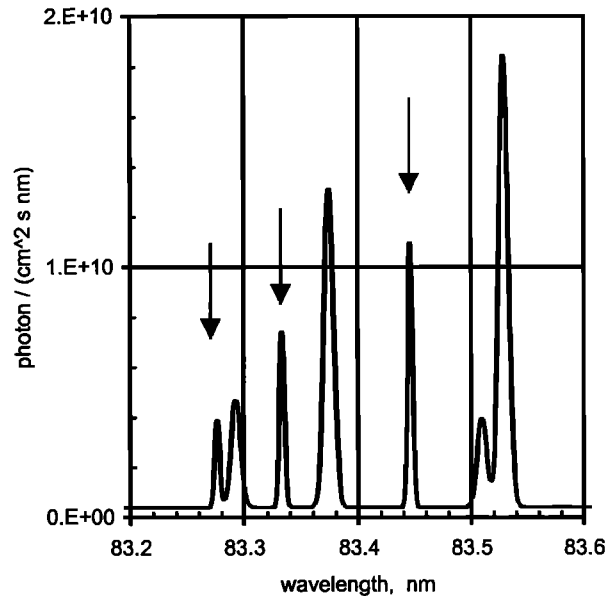
Figure 4. Solar irradiance model in the vicinity of 83.4 nm used in this work. Arrows mark the O II triplet lines; other lines are of the O III multiplet. One can see that the Doppler shift effects could be significant and require accurate calculations.

vicinity (< 5 AU), where many important pickup ions originate, is limited in the two-shock model. For the purposes of our work, the interstellar gas properties inside the termination shock can be reliably calculated using the hot model with the modified LISM parameters "at infinity" [*Gruntman*, 1992b, 1994].

The Saha ionization formula applied to the most believed LISM parameters, $n \sim 0.1$ cm^{-3} and $T \approx 7000$ K, would give the fractional ionization of hydrogen $\xi_H \sim 0.01$. This result contrasts with many observational indications of much higher local electron densities [e.g., *Cox and Reynolds*, 1987; *Frisch*, 1990, 1995; *Reynolds*, 1990; *Breitschwerdt*, 1996; *Vallerga*, 1998]. The LISM is not in a state of thermodynamical equilibrium, and its stationary ionization state is determined by a balance of the processes of ionization and recombination. The ionization state of interstellar oxygen, a minor component of the LISM, is determined by the ionization state of hydrogen [*Field and Steigman*, 1971; *Fahr et al.*, 1995].

4. Solar 83.4 nm Radiation and *g* factor

An oxygen O$^+$ ion has a triplet transition at 83.2754, 83.3326, and 83.4462 nm [e.g., *Meier*, 1990]. Both solar emission O$^+$ and O^{++} multiplets could excite interstellar and heliospheric O$^+$ ions. Accurate knowledge of the relative strengths and line widths of these solar emissions is indispensable for calculations of the *g* factors. The properties of the full solar disk emission at 83.4 nm were poorly known until *Meier* [1990] found and analyzed the old Aerobee-Hi rocket measurements performed by a Naval Research Laboratory group on August 22, 1962 [*Tousey et al.*, 1963].

The solar irradiance model used in this work is shown in Figure 4. This model (D. Shemansky, private communications, 1997) closely reproduces the measured solar spectral distribution [*Meier*, 1990]. The arrows mark the O II triplet lines; the other lines belong to the O III multiplet. The contributions of the different solar lines to O$^+$ excitation would
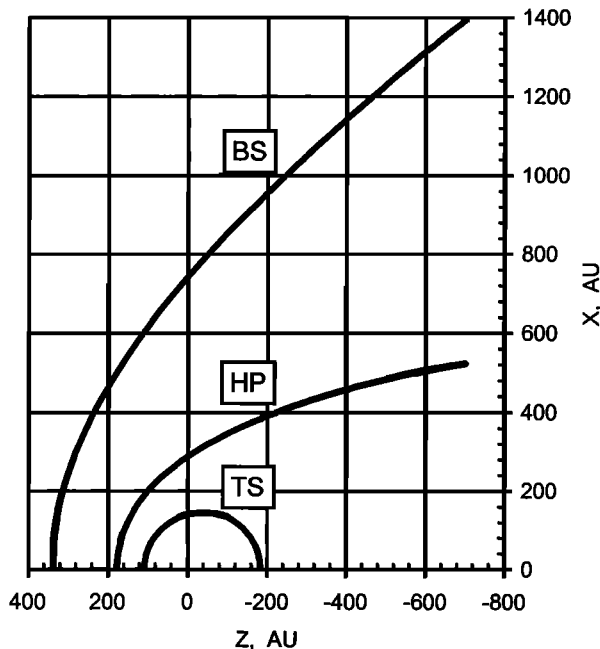

Figure 3. The axis-symmetric heliospheric structure used in this work (calculations by Vladimir Baranov and his group, 1997). The interstellar wind approaches from the left along the *Z* axis. BS, bow shock, HP, heliopause, TS, termination shock. The Sun is at the (0,0) point.

strongly depend on the individual ion velocity. For example, an ion radial velocity of 300 km s^{-1} would correspond to a Doppler shift of ~0.08 nm. Typical radial velocities of the LISM plasma vary between ±30 km s^{-1} (Doppler shifts of ±0.008 nm), while typical radial velocities of pickup ions in the solar wind vary from 0 to 1000 km s^{-1} (Doppler shifts of 0–0.28 nm). The total solar photon flux in all the lines (Figure 4) is 5.30×10^8 cm^{-2} s^{-1} at 1 AU; the continuum is ~4.0×10^8 cm^{-2} s^{-1} nm^{-1}. The adopted line emission is ~25% smaller than the 6.7×10^8 cm^{-2} s^{-1} value given by Meier [1991] on the basis of measurements by Hinteregger et al. [1981] for the solar minimum conditions. Our solar line model assumption would thus lead to conservative estimates of the LISM glow.

Let us consider a Maxwellian gas of particles (ions) with the temperature T and radial bulk flow velocity V_B with respect to the Sun. The gas is illuminated by the solar radiation with the spectral distribution $F(\lambda)$ cm^{-2} s^{-1} nm^{-1}. The effective excitation scattering rate per particle per second, the g factor $g(V_B,T)$, at the transition wavelength λ_0 can be obtained by integrating the expression (weighted by the Maxwellian distribution) for a g factor with a continuum excitation source over the spectral range of interest

$$g(V_B,T) \quad (3)$$

$$= \left[\frac{\pi e^2}{mc} f \frac{\lambda_0^2}{c} F(\lambda) \frac{1}{U\sqrt{\pi}} \frac{c}{\lambda_0} \exp\left[-\frac{\left(\frac{c(\lambda-\lambda_0)}{\lambda_0} + V_B \right)^2}{U^2} \right] d\lambda, \right.$$

where f is the transition oscillator strength; m and e are the electron mass and charge, respectively; and c is the speed of light. The most probable particle (ion) velocity U in the gas is

$$U = \left(\frac{2k_B T}{M} \right)^{1/2}, \quad (4)$$

where k_B is the Boltzmann constant and M is the particle (ion) mass.

We verified the solar irradiance model and other computer codes developed for this work by reproducing the O$^+$ ion g factor dependences on gas temperature and bulk velocity, first calculated by Meier [1990]. For example, the total g factor (at 1 AU) is 1.29×10^{-6} s^{-1} for a gas of oxygen ions with a temperature of 0.1 eV (11,605 K) at rest, with the radiation continuum contributing ~5% of the scattering rate (glow) of the ions.

5. Sky background and foreground at 83.4 nm

There are two other major sources of radiation at 83.4 nm, namely, diffuse galactic radiation (background) and the solar radiation resonantly scattered by the O$^+$ ions within the heliopause boundary (foreground). Various theoretical estimates and observations indicate that the galactic continuum background does not exceed 4×10^{-5} R nm^{-1} (4×10^{-6} R Å^{-1}) [Paresce and Jakobsen, 1980; Cheng and Bruhweiler, 1990; Vallerga and Welsh, 1995; Vallerga, 1996, 1998] in the 80-86 nm spectral range. The photometric unit Rayleigh is defined as 1 R = (10^6/4π) photon (cm^2 s sr)$^{-1}$; one micro-Rayleigh 1μR = 10^{-6} R would correspond to the flux of ~0.08 photon (cm^2 s sr)$^{-1}$. The heliopause-reflected EUV radiation is line emissions,

which simplifies their separation from the continuum background. The galactic O$^+$ resonance line emission is believed to be negligible [Cheng and Bruhweiler, 1990].

The galactic continuum background in EUV is essentially anisotropic. It was recently discovered that a nearby B2 II star, ε Canis Majoris (Adhara/Adara), is responsible for most of the background in this spectral range. This star is located at ecliptic longitude 110.7° and ecliptic latitude –51.4°. Earth is in the projection of the direction from the Sun to this star in early January each year (Figure 5). The sky background in the directions other than toward ε Canis Majoris could be several times lower than the average background. Thus the galactic background at 83.4 nm could be assumed to be $\lesssim$ 1×10^{-5} R nm^{-1} (1 μR Å^{-1}) as long as one does not point the instrument in the direction of ε Canis Majoris.

Neutral interstellar atoms penetrate the heliosphere where they are ionized and carried to the termination shock as pickup ions [Moebius et al., 1985; Gloeckler et al., 1993; Moebius, 1996]. The pickup ions are singly charged and characterized by a spherical shell velocity distribution function. The O$^+$ pickup ions would resonantly scatter the solar radiation, producing the foreground "glow." Contrary to the galactic background, solar radiation scattered by both the LISM plasma and the pickup ions are line emissions, with their relative intensities being most important for determining the feasibility of heliopause mapping. The pickup ion glow can be calculated by applying (1).

The local production rate of heliospheric oxygen O$^+$ ions is $\alpha(R,\theta) = \beta(R) \times N_0(R,\theta)$, where $\beta(R)$ is the atomic oxygen ionization rate and $N_0(R,\theta)$ is the local number density of neutral atomic oxygen. Oxygen ionization occurs predominantly by photoionization and charge exchange with the solar wind protons. We assume that both the solar EUV
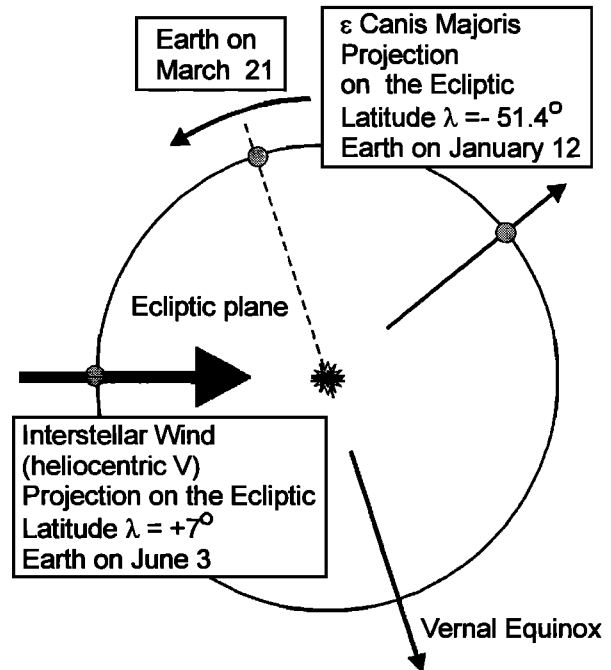

Figure 5. The star ε Canis Majoris is the major source of galactic background, estimated to be 4×10^{-5} R nm^{-1}, at 83.4 nm. The background could be safely assumed to be <10^{-5} R nm^{-1} in the directions other than that of ε Canis Majoris.

radiation and the solar wind flow are isotropic and that oxygen ionization can be described as $\beta(R) = \beta_E (R_E/R)^2$, where β_E is the ionization rate at $R_E = 1$ AU.

The photoionization rate is assumed to be 3.2×10^{-7} s^{-1} at 1 AU [*Izmodenov et al., 1997*]. The charge exchange rate is 2.6×10^{-7} s^{-1} for the solar wind speed $V_{SW} = 450$ km s^{-1} and number density (at 1 AU) $n_{SW} = 7$ cm^{-3} assumed in this work; the charge exchange cross section at this collision velocity is 8.2×10^{-16} cm^{-2}. The total oxygen ionization rate is $\beta_E = 5.8 \times 10^{-7}$ s^{-1}.

The expanding solar wind flow gradually slows down due to mass loading and loss of momentum and energy in charge exchange. However, one can safely disregard this process in glow calculations because (see Section 7) most of the 83.4-nm radiation is produced in the region within 10 AU from the Sun, where the effect of the solar wind slowing down is small.

We assume that the oxygen ions are instantaneously picked up by the solar wind plasma. The number density of the oxygen pickup ions at a given point R_0 can be calculated by dividing the local flux F_{O+} of the pickup ions by the solar wind speed [*Gruntman*, 1992b]:

$$N_{O+}(R_0,\theta) = \frac{F_{O+}(R_0,\theta)}{V_{SW}}$$

$$= \frac{1}{V_{SW}} \int_{R_S}^{R_0} \beta_E \left(\frac{R_E}{R}\right)^2 N_O(R,\theta) \left(\frac{R}{R_0}\right)^2 dR \quad (5)$$

$$= \frac{\beta_E}{V_{SW}} \left(\frac{R_E}{R_0}\right)^2 \int_{R_S}^{R_0} N_O(R,\theta) dR .$$

The pickup ion flux is determined by an integral from the Sun's surface R_S to the observation point R_0, where the $(R_E/R)^2$ factor describes the radial dependence of the total oxygen ionization rate and the $(R/R_0)^2$ factor describes pickup ion number density decrease because of the radial expansion of the solar wind. The number density of the neutrals is usually negligible close (< 0.1 AU) to the Sun. Therefore the assumption of the constant solar wind speed, which does not hold in the Sun's close vicinity, does not introduce a significant error.

Neutral interstellar oxygen distribution $N_O(R,\theta)$ was calculated using the hot model of the interstellar gas inflow into the heliosphere [e.g., *Fahr*, 1974; *Holzer*, 1977; *Thomas*, 1978]. Interstellar neutral oxygen, similarly to hydrogen and contrary to helium, is significantly affected by the charge exchange processes in the heliospheric interface. The interactions in the interface result in the slowing of the interstellar gas flow (effective velocity decrease) and widening of the velocity distribution function (effective temperature increase) [*Baranov and Malama*, 1993; *Lallement et al.*, 1993; *Fahr*, 1996; *Kausch and Fahr*, 1997; *Izmodenov et al.*, 1997]. We modeled [*Gruntman*, 1992b, 1994] the neutral oxygen distribution using the hot model with the oxygen loss rate 5.8×10^{-7} s^{-1} at 1 AU and the following interstellar gas parameters at infinity: velocity 20 km s^{-1}, temperature 12,000 K. It was assumed that 75% (filtering coefficient) of oxygen atoms pass the interface region without loss [*Izmodenov et al.*, 1997].

The pickup ion glow, as seen from 1 AU, is described by (1) with integration from the observation point R_E to the termination shock $R_{TS}(\theta)$. We assume that the pickup ions

instantaneously form a spherical shell in the velocity space moving with the solar wind speed. The velocity vectors of all pickup ions (in the reference frame of the solar wind flow) have the same magnitude (equal to that of the solar wind V_{SW}) and pointed isotropically. Because of the assumption of the constant solar wind speed the pickup ion velocity distribution function does not change its shape as the solar wind expands. An ion velocity radial component V_R determines the Doppler shift. For a spherical shell velocity distribution function, the distribution function $f(V_R)$ is flat in the 0 to $(2V_{SW})$ velocity range in the reference frame with the Sun at rest and equals zero outside this range. The pickup ion g factor would thus be inversely proportional to the distance to the Sun (under the optically thin conditions), and (1) can be simplified as follows

$$F_{SW}(\theta) = \frac{g_E R_E^2}{4\pi} \int_{R_E}^{R_{TS}} \frac{N_{O+}(R,\theta)}{R^2} dR. \quad (6)$$

The pickup ion g factor dependence on the solar wind speed at 1 AU is shown in Figure 6. It is important that the solar spectrum continuum significantly contributes to the pickup ion glow and has to be accurately accounted for in the calculations.

6. Sky Brightness at 83.4 nm

The sky brightness at 83.4 nm includes the glow of the LISM plasma beyond the heliopause, the pickup ion glow foreground, and the diffuse galactic continuum background. The calculated directional dependences of the 83.4-nm glow of the LISM plasma F_{LISM} and the solar wind pickup ions F_{SW} are shown in Figure 7. The solid curve is a function $1/R_{HP}(\theta)$ normalized at $\theta = 0$.

The initial slight increase of the LISM plasma brightness with the angle θ is due to the Doppler effect as the velocity radial component diminishes in the plasma flowing around the heliopause. The brightness falls as the heliopause moves farther away from the Sun and the Doppler effect reduces the g factor.
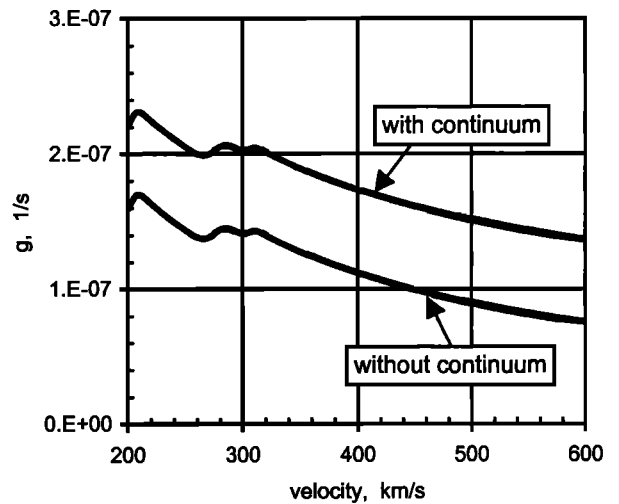
Figure 6. Solar wind oxygen pickup ion scattering rate (g factor) at 1 AU as a function of the solar wind velocity for the solar line emissions only (without continuum) and for the total solar emissions (lines and continuum). Solar radiation continuum significantly contributes to the pickup ion glow.
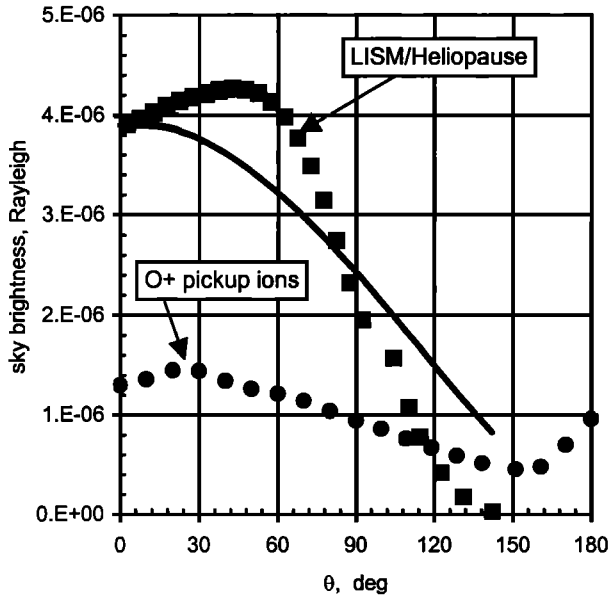
Figure 7. Glow at 83.4 nm of the LISM plasma beyond the heliopause and the solar wind pickup ions. The solid curve is a function $1/R_{HP}(\theta)$ normalized at $\theta = 0$; R_{HP} is the distance to the heliopause.

If the LISM plasma had constant number density, temperature, and velocity, then its glow angular dependence would have been described, according to (2), by the solid curve. The difference between the solid curve and the calculated LISM plasma glow shows the sensitivity of heliopause imaging to the plasma flow field beyond the heliopause.

The pickup ion glow is determined by the distribution of oxygen in the heliosphere. The glow increase in the downwind region ($\theta = 180°$) is a result of gravitational focusing of the inflowing interstellar neutral atoms with the corresponding increase of the pickup ion number density in this direction.

The $F_{LISM}(\theta)$ and $F_{SW}(\theta)$ dependences (Figure 7) were calculated under the assumption that the interstellar oxygen ionization degree is exactly the same as that of the LISM n_e/n_H = 1/2 ($n_e = 0.07$ cm^{-3}, $n_H = 0.14$ cm^{-3}). The brightness of the LISM plasma is roughly proportional to the number density of the interstellar gas ionized component, while the pickup ion brightness is roughly proportional to the number density of the interstellar gas neutral component. For example, an increase in the LISM ionization degree would result in an increase of the F_{LISM}/F_{SW} ratio. One can scale F_{LISM} and F_{SW} with the number densities of the LISM ionized and neutral components, respectively, in order to evaluate the sky map dependence on the LISM ionization state.

Figure 8 demonstrates the total sky brightness ($F_{LISM} + F_{SW}$) directional dependences for various ionization states of the LISM obtained by simple scaling of the dependences in Figure 7: $n_e/n_H=1/2$, $n_e/n_H=1$, $n_e/n_H=2$, the total LISM number density is 0.21 cm^{-3}. The upwind-to-downwind brightness ratios are 5.4, 9.4, and 17.5, respectively, and show strong dependence on the LISM ionization degree. The corresponding sky maps at 83.4 nm are shown in Plate 1 in the ecliptic coordinates (Mercator projection), with color coding of sky brightness. These images are representative of the sky maps that would be obtained in a heliopause imaging experiment after subtraction of the diffuse galactic background. The sky brightness peaks in the upwind

direction (ecliptic longitude 252° and latitude +7°) for the interstellar gas flow relative to the sun. The secondary peak in the downwind direction produced by the oxygen pickup ions is obscured by the selected color palette and better seen in Figure 8.

7. Discussion

The sky glow angular dependences are essentially different for the LISM plasma beyond the heliopause ($F_{LISM}(\theta)$) and pickup ions ($F_{SW}(\theta)$). Therefore mapping the sky at 83.4 nm is a direct way to establish the relative contributions of F_{LISM} and F_{SW} and thus the ionization state of interstellar oxygen and hydrogen. While the sky brightness from the upwind direction is determined by both the interstellar plasma and pickup ion glows, the sky brightness in the downwind direction ($\theta=180°$) is almost exclusively attributed to the pickup ions. The interstellar magnetic field would result in additional LISM pressure leading to a smaller heliosphere, with the resulting increase of the heliopause brightness F_{LISM}.

Simple scaling of the sky brightness (Figure 8) with the interstellar plasma and gas number densities is not quantitatively precise because the position and shape of the heliopause and other heliospheric surfaces would also depend on the LISM ionization degree, even for the same total LISM number density. In addition, plasma-gas charge exchange coupling is a nonlinear effect. This scaling is useful, however, to demonstrate the expected trends in sky images and their sensitivity to the LISM ionization state.

For the lowest considered LISM ionization degree, $n_e/n_H=1/2$, the expected heliopause (LISM plasma) brightness is significantly higher than that of the pickup ion glow in the upwind direction (Figures 7 and 8). The interstellar plasma and pickup ion glows would be about the same at $n_e/n_H \approx 1/8$. The pickup ion glow would always dominate the sky brightness in the downwind direction.
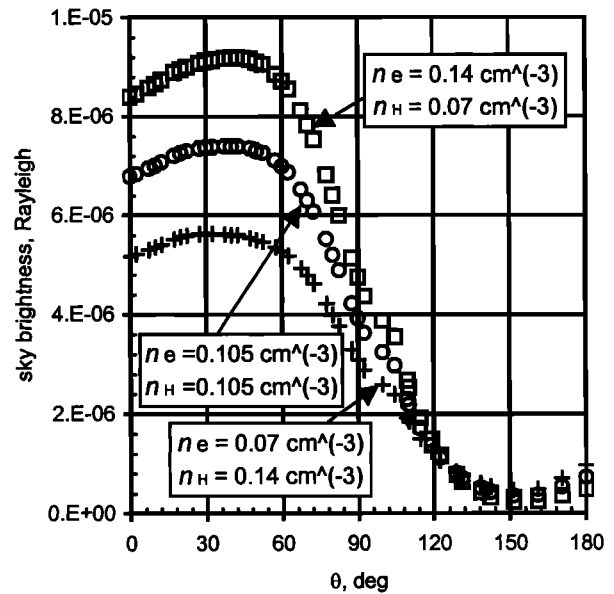

Figure 8. Total sky brightness ($F_{LISM} + F_{SW}$) directional dependences for various ionization states of the LISM: $n_e/n_H=1/2$; $n_e/n_H=1$; $n_e/n_H=2$. The curves are obtained by scaling of the dependences in Figure 7; the total LISM number density is 0.21 cm^{-3}.
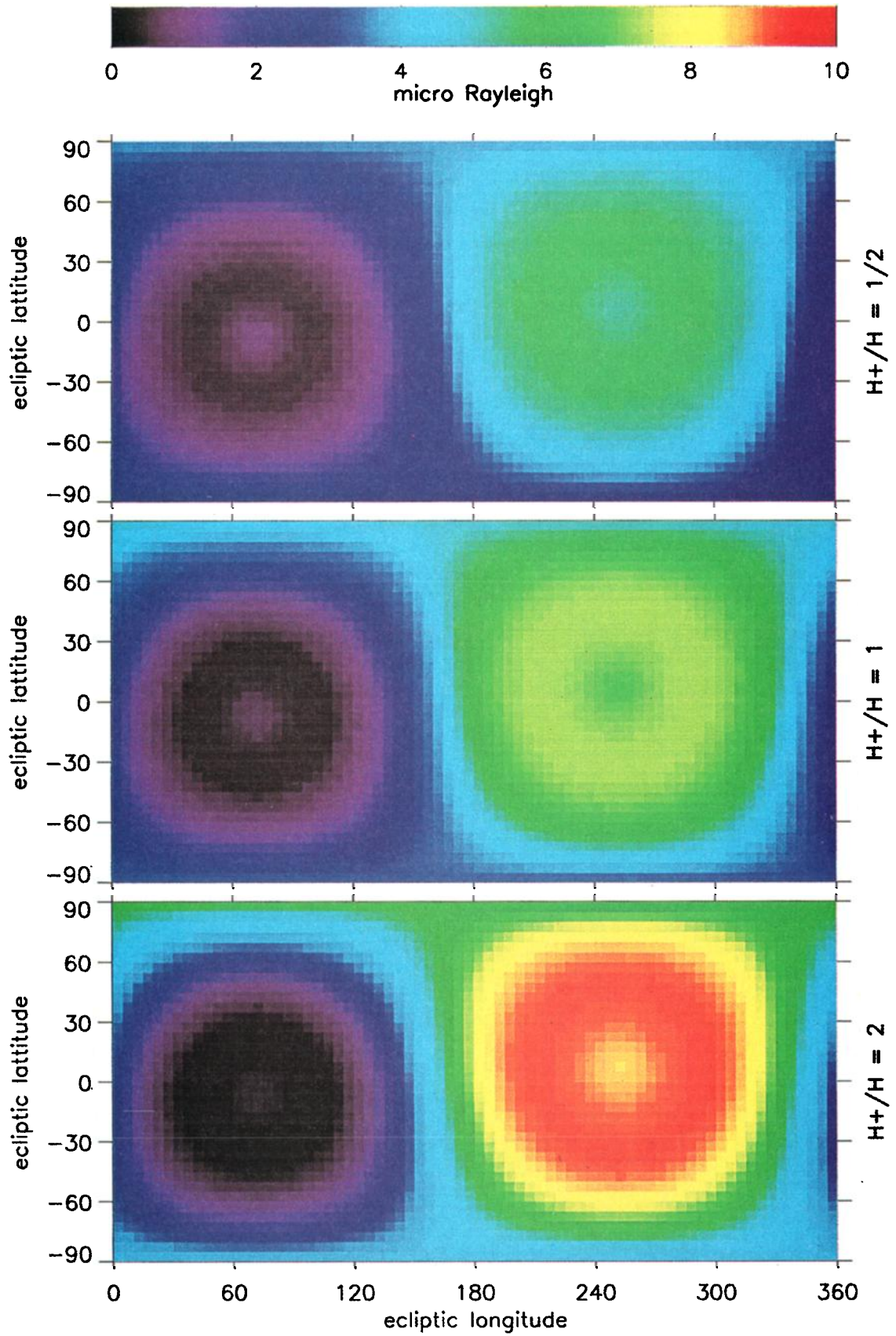
Plate 1. All-sky images (ecliptic coordinates) of the sky brightness at 83.4 nm for various ionization states of the LISM: (top) n_e/n_H=1/2, (middle) n_e/n_H=1, (bottom) n_e/n_H=2, the total LISM number density is 0.21 cm^{-3}.

The heliopause shape and the LISM plasma flow field are sensitive to the interstellar magnetic field. The tilt of the magnetic field vector with respect to the interstellar wind velocity vector would result in an asymmetric heliopause and termination shock. The shape of the termination shock can be sensed by ENA global imaging: however, the asymmetry would be much more strongly pronounced for the heliopause than for the termination shock. Heliopause EUV mapping would open a promising way for remote probing of the asymmetry of the LISM magnetic field.

Solar wind latitudinal asymmetry [*McComas et al.*, 1998] is important in determining the shape of the heliopause. The solar wind-produced asymmetry would be strongly pronounced in the shape of the termination shock as well (Gruntman et al., manuscript in preparation, 2000). Termination shock ENA imaging and heliopause EUV imaging are a powerful combination of the complementary remote techniques to probe asymmetry of the heliosphere and separate the effects of the solar wind and the interstellar magnetic field.

Solar wind pickup ions along the line of sight contribute to the observed glow. The glow source functions $(N_{O+}(R)/R^2)$ for the upwind (θ = 0) and downwind (θ = 180°) directions are shown in Figure 9. One can see that most of the glow originates within 10 AU from the Sun, which justifies the simplifying assumption of the solar wind constant speed. The pickup ion glow as a function of the position of an observer is shown in Figure 10 for the upwind direction. The glow is almost a factor of 2 smaller at 2 AU and a factor of 5 at 5 AU. The glow measurements performed farther than 1 AU from the Sun would provide "cleaner" maps of the LISM plasma glow.

Planets also contribute to the neutral oxygen population in the heliosphere. Jupiter is the most important non-LISM source of heliospheric oxygen [*Luhmann*, 1994]. Jupiter's magnetosphere emits energetic oxygen atoms with the speed $V_{O-J} \approx 75$ km s^{-1}. The total atom flux from this source is Φ_{O-J} = $(1-5)\times10^{28}$ s^{-1} [*Eviatar and Barbosa*, 1984; *Cheng*, 1986; *Barbosa and Eviatar*, 1986; *Luhmann*, 1994]. Assuming

Figure 10. Pickup ion glow as a function of the position of an observer for the upwind direction.

isotropic emission of oxygen and disregarding losses, the number density of Jupiter-produced oxygen atoms, N_{O-J}, would be

$$N_{O-J}(r) = \frac{\Phi_O}{4\pi r^2 V_{O-J}}, \tag{7}$$

where r is the distance from Jupiter.

The calculated number densities of interstellar oxygen atoms $N_O(R)$ and O$^+$ pickup ions $N_{O+}(R)$ in the upwind direction (θ = 0) are shown in Figure 11. Neutral interstellar oxygen would dominate everywhere beyond the distance of ~0.2 AU from Jupiter. Jupiter is at 5.2 AU from the Sun, and the expected interstellar oxygen number density is ~5×10^{-5} cm^{-3} at this location. The number density of the Jupiter-produced oxygen pickup ions can be obtained by applying (5) and replacing
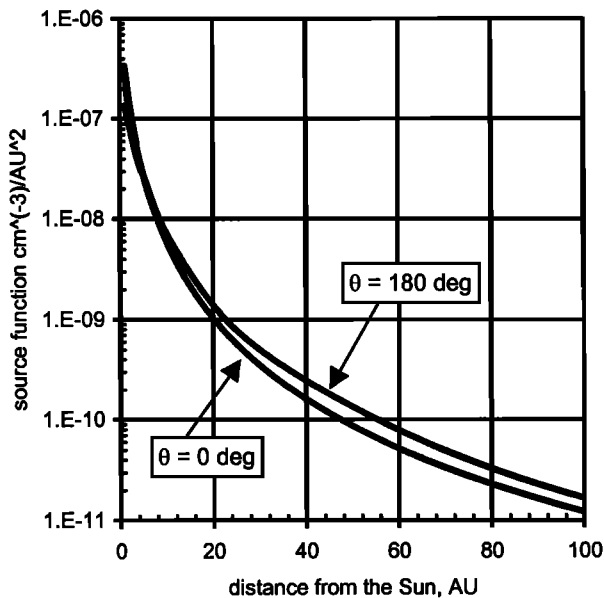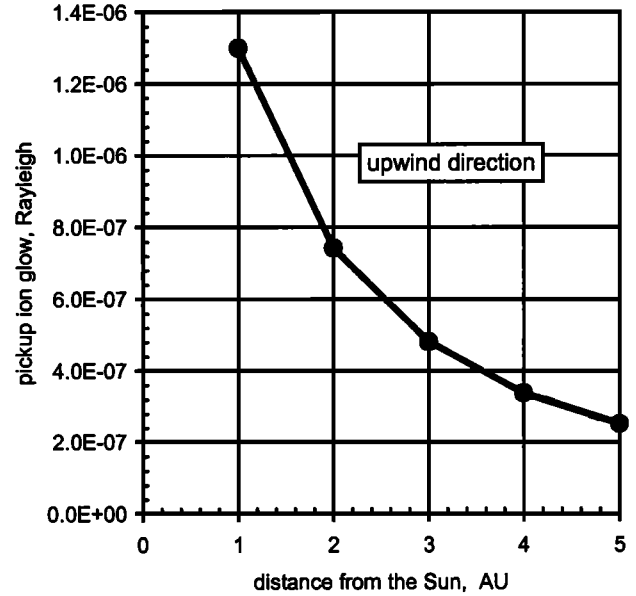

Figure 9. Oxygen pickup ion glow source functions $(N_{O+}(R)/R^2)$ for the upwind (θ = 0) and downwind (θ = 180°) directions.
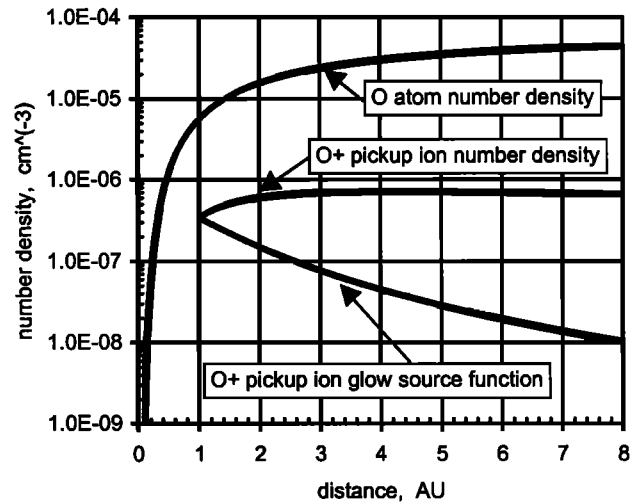

Figure 11. Neutral density radial dependence of interstellar oxygen atoms $N_O(R)$ and O$^+$ pickup ions $N_{O+}(R)$ in the upwind direction (θ = 0). Also shown is the O$^+$ pickup ion glow source function $N_{O+}(R)/R^2$ cm^{-3} AU^{-2}.

$N_0(R)$ by $N_{O,J}(R)$. Pickup ions of interstellar origin (the number density is $\sim 8 \times 10^{-7}$ cm^{-3} at 5.2 AU) would dominate everywhere beyond the distance of 0.5 AU from Jupiter.

The interstellar pickup ion glow source function $N_{O+}(R)/R^2$ cm^{-3} AU^{-2} is also shown in Figure 11. The contribution of interstellar ions from within the 1-AU sphere around Jupiter does not exceed 5% of the total interstellar pickup ion glow as seen from 1 AU. Therefore the Jupiter-produced pickup ions would contribute only a few percent of the total pickup ion glow when observed directly at Jupiter. The Jupiter-produced increase in the pickup ion glow would be noticeable only within a field of view of a few degrees centered on the planet.

We assumed isotropic oxygen emission from Jupiter in our estimate. The expected anisotropy of the oxygen emission (oxygen energetic neutral atom "thermal" speed is ~ 13 km s^{-1} [Cheng, 1986]) would result in an increase of this relatively bright area up to $\pm 5°$. Thus Jupiter does not pose an obstacle for heliopause mapping in EUV. The sky map pixels with Jupiter and ε Canis Majoris should be disregarded or used for calibration purposes.

The LISM plasma and pickup ion glow spectral properties are significantly different. Figure 12a shows the calculated LISM plasma glow spectral distribution for the approximately upwind direction ($\theta = 2.5°$). The spectral distribution of the pickup ion glow, which is independent of the direction of observation, is shown in Figure 12b. More than half of the LISM plasma-scattered radiation is concentrated at 83.45 nm, while most of the pickup ion-scattered radiation is at <83.40 nm. This difference in the spectral properties of radiation can be used to further distinguish between the LISM and pickup ion-produced glows and to explore the velocity distribution of pickup ions and the flow field of the LISM plasma.

A heliopause EUV imaging experiment would require a modest spectral resolution, ~ 0.01-0.1 nm, while the required ~ 1 μR sensitivity is a challenge. A spectral resolution of 0.2 nm (2 Å) would allow one to detect the LISM plasma and pickup ion glow and separate them from the diffuse galactic background. A better resolution, ~ 0.02 nm (0.2 Å), would allow separation of the LISM plasma and pickup ion glows (Figure 12). The recently developed new EUV spectrometers have significantly advanced the art of diffuse EUV radiation detection, achieving the sensitivity of ~ 10 mR nm^{-1} (1 mR Å^{-1}) [Bowyer et al., 1997]. Heliopause mapping would further require 3 orders of magnitude improvement. This is a challenging but not impossible task.

The heliopause mapping experiment and instrument are beyond the scope of this article. We only note that the successfully demonstrated diffuse EUV spectrometer [Bowyer et al., 1997] can serve as a solid foundation for further development. The required characteristics could be achieved by maximizing diffraction grating reflection at 83.4 nm and improving suppression of radiation diffuse scattering in the bright 121.6-nm and 58.4-nm lines. Heliospheric diffuse 121.6-nm and 58.4-nm line emissions may be as bright as ~ 1000 R and ~ 10 R, respectively, and their suppression is an important spectrometer requirement. An imaging photon-counting detector requires maximum detection efficiency at 83.4 nm, while suppressing detection at 121.6 nm. The efficiency of the anticoincidence noise rejection technique [Bowyer et al., 1997] should also be further improved.

Heliopause EUV mapping can be performed only from a spacecraft well outside the geocorona. An obvious experiment
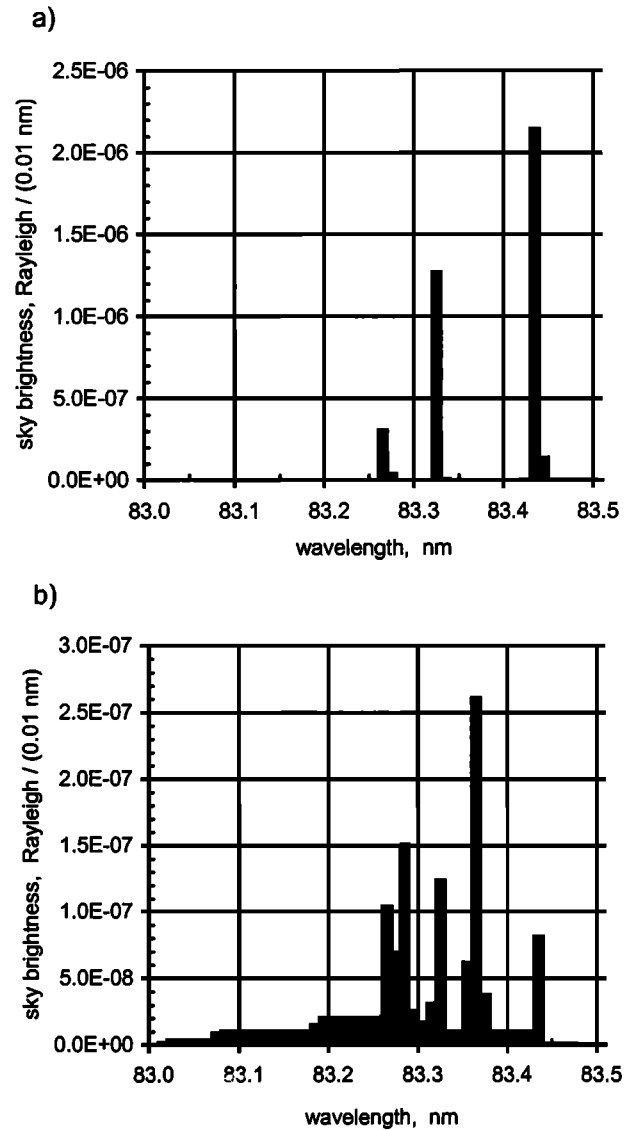
a)

b)

Figure 12. (a) Spectral distribution (0.01-nm = 0.1-Å bins) of the glow of the LISM plasma beyond the heliopause. (b) Spectral distribution of the oxygen pickup ion glow. Note the difference in vertical scales.

requirement is to obtain an all-sky map within the lifetime of a typical mission, i.e., within 3-5 years. A composite heliopause map would be produced by an instrument with a single, or a few imaging pixels. If it takes an instrument ~ 1 week to detect photons with the desired statistical accuracy in one pixel, then the whole sky can be covered by $\sim 30° \times 30°$ pixels in 1 year, or by $\sim 13° \times 13°$ pixels in a typical 5-year mission lifetime. A high-speed instrument measuring one pixel per day would cover the entire sky by $\sim 10° \times 10°$ pixels in 1 year. Statistical accuracy of 3% would require accumulation of ~ 1000 counts of the reflected solar 83.4-nm photons per pixel.

For a spinner spacecraft a combination of the instrument axis spinning and precession of the spin axis could achieve the sky coverage. An all-sky image could be conveniently accumulated in half a year in such a mode of operation. Scarcity of photons would require a combination of several all-sky scans with gradually improving statistical accuracy as the mission progresses. As always, it is highly desirable to minimize the

resources required for the mission. A preliminary analysis shows that a near-Earth, outside of the geocorona, space mission could be the best choice for the resource-limited heliopause imaging experiment (M. Gruntman, unpublished manuscript, May 1997).

References

Axford, W.I., The interaction of the solar wind with the interstellar medium, in *Solar Wind*, edited by C.P. Sonnett, P.J. Coleman, and J.M. Wilcox, *NASA Spec. Publ., NASA SP-308*, 609-660, 1972.

Axford, W.I., Interaction of the solar wind with the interstellar medium, in *Physics of the Outer Heliosphere*, edited by. S. Grzedzielski and D.E. Page, pp. 7-15, Pergamon, Tarrytown, N.Y., 1990.

Baranov, V.B., and Y.G. Malama, The model of the solar wind interaction with the local interstellar medium: Numerical solution of self-consistent problem, *J. Geophys. Res.*, 98, 15,157-15,163, 1993.

Baranov, V.B., and Y.G. Malama, Effect of interstellar medium hydrogen fractional ionization on the distant solar wind and interface region, *J. Geophys. Res.*, 100, 14,755-14,761, 1995.

Baranov, V.B., V.V. Izmodenov, and Y. G. Malama, On the distribution function of H atoms in the problem of the solar wind interaction with the local interstellar medium, *J. Geophys. Res.*, 103, 9575-9585, 1998.

Barbosa, D.D., and A. Eviatar, Planetary fast neutral emissions and effects on the solar wind: A cometary exosphere analog, *Astrophys. J.*, 310, 927-936, 1986.

Bertaux, J.-L, Helium and hydrogen of the local interstellar medium observed in the vicinity of the Sun, in *IAU Colloquium 81, NASA Conf. Publ., NASA CP 2345*, 3-23, 1984.

Bowyer, S., J. Edelstein, and M. Lampton, Very high sensitivity extreme ultraviolet spectrometer for diffuse radiation, *Astrophys. J.*, 485, 523-532, 1997.

Breitschwerdt, D., The local bubble, *Space Sci. Rev.*, 78, 173-182, 1996.

Chakrabarti, S., F. Paresce, S. Bowyer, Y.T. Chiu, and A. Aikin, Plasmaspheric helium ion distribution from satellite observations of He II 304-Å, *Geophys. Res. Lett.*, 9, 151-154, 1982.

Chakrabarti, S., R. Kimble, and S. Bowyer, Spectroscopy of the EUV (350-1400 Å) nightglow, *J. Geophys. Res.*, 89, 5660-5664, 1984.

Cheng, A.F., Energetic neutral particles from Jupiter and Saturn, *J. Geophys. Res.*, 91, 4524-4530, 1986.

Cheng, K.-P., and F.C. Bruhweiler, Ionization processes in the local interstellar medium: Effects of the hot coronal substrate, *Astrophys. J.*, 364, 573-581, 1990.

Cox, D.P., and R.J. Reynolds, The local interstellar medium, *Annu. Rev. Astron. Astrophys.*, 25, 303-344, 1987.

Davis, L, Jr., Interplanetary magnetic field and cosmic rays, *Phys. Rev.*, 100, 1440-1444, 1955.

Dessler, A. J., Solar wind and interplanetary magnetic field, *Rev. Geophys.*, 5, 1-41, 1967.

Dupuis, J., S. Vennes, S. Bowyer, A.K. Pradhan, and P. Thejll, Hot white dwarfs in the local interstellar medium: Hydrogen and helium interstellar column densities and stellar effective temperatures from Extreme-Ultraviolet Explorer spectroscopy, *Astrophys. J.*, 455, 574-589, 1995.

Eviatar, A., and D.D. Barbosa, Jovian magnetospheric neutral wind and auroral precipitation flux, *J. Geophys. Res.*, 89, 7393-7398, 1984.

Fahr, H.J., The extraterrestrial UV-background and the nearby interstellar medium, *Space Sci. Rev.*, 15, 483-540, 1974.

Fahr, H.J., The interstellar gas flow through the heliospheric interface region, *Space Sci. Rev.*, 78, 199-212, 1996.

Fahr, H.J., and H. Fichtner, Physical reasons and consequences of a three-dimensionally structured heliosphere, *Space Sci. Rev.*, 58, 193-258, 1991.

Fahr, H.J., R. Osterbart, and D. Rucinski, Modulation of the interstellar oxygen-to-hydrogen ratio by the heliospheric interface plasma, *Astron. Astrophys.*, 294, 587-600, 1995.

Field, G.B., and G. Steigman, Charge transfer and ionization equilibrium in the interstellar medium, *Astrophys. J.*, 166, 59-64, 1971.

Frisch, P. C., Characteristics of the local interstellar medium, in *Physics of the Outer Heliosphere*, edited by S. Grzedzielski and D. E. Page, pp. 19-28, Pergamon, Tarrytown, N.Y., 1990.

Frisch, P. C., Characteristics of nearby interstellar medium, *Space Sci. Rev.*, 72, 499-592, 1995.

Frisch, P.C., and J.D. Slavin, Relative ionizations in the nearest interstellar gas, *Space Sci. Rev.*, 78, 223-228, 1996.

Gloeckler, G., J. Geiss, H. Balsiger, L. A. Fisk, A. B. Galvin, F. M. Ipavich, K. W. Ogilvie, R. von Steiger, and B. Wilken, Detection of interstellar pickup hydrogen in the solar system, *Science*, 261, 70-73, 1993.

Gruntman, M.A., Anisotropy of the energetic neutral atom flux in the heliosphere, *Planet. Space Sci.*, 40, 439-445, 1992a.

Gruntman, M.A., Charge-exchange born He^+ ions in the solar wind, *Geophys. Res. Lett.*, 19, 1323-1326, 1992b.

Gruntman, M.A., Neutral solar wind properties: Advance warning of major geomagnetic storms, *J. Geophys. Res.*, 99, 19213-19227, 1994.

Gruntman, M.A., Energetic neutral atom imaging of space plasmas, *Rev. Sci. Instrum.*, 68, 3617-3656, 1997.

Gruntman, M.A., and H.J. Fahr, Access to the heliospheric boundary: EUV-echoes from the heliopause, *Geophys. Res. Lett.*, 25, 1261-1264, 1998.

Gruntman, M.A, E.C. Roelof, D.G. Mitchell, H.O. Funsten, D.J. McComas, and H.-J. Fahr, Energetic neutral atom imaging of the heliospheric termination shock and interface region on an "Interstellar Pathfinder" mission, *Eos Trans. AGU*, 80(17), Spring Meet. Suppl., S237, 1999.

Gurnett, D.A., and W.S. Kurth, Radio emissions from the outer heliosphere, *Space Sci. Rev.*, 78, 53-66, 1996.

Hilchenbach, M., et al., Detection of 55-80 keV hydrogen atoms of heliospheric origin by CELIAS/HSTOF on SOHO, *Astrophys. J.*, 503, 916-922, 1998.

Hinteregger, H., K. Fukui, and B.R. Gilson, Observational, reference, and model data on solar EUV, from measurements on AE-E, *Geophys. Res. Lett.*, 8, 1147-1150, 1981.

Holzer, T.E., Neutral hydrogen in interplanetary space, *Rev. Geophys.*, 15, 467-490, 1977.

Hsieh, K.C. and M.A. Gruntman, Viewing the outer heliosphere in energetic neutral atoms, *Adv. Space Res.*, 13(6), 131-139, 1993.

Izmodenov, V., Y.G. Malama, and R. Lallement, Interstellar neutral oxygen in a two-shock heliosphere, *Astron Astrophys.*, 317, 193-202, 1997.

Kausch, T., and H.J. Fahr, Interstellar gas filtration to the inner heliosphere under self-consistent influence of a pickup ion modulated termination shock, *Astron. Astrophys.*, 325, 828-838, 1997.

Lallement, R., J.-L. Bertaux, and J.T. Clarke, Deceleration of interstellar hydrogen at the heliospheric interface, *Science*, 260, 1095-1098, 1993.

Liewer, P.C., R.A. Mewaldt, J.A. Ayon, and R.A. Wallace, NASA's Interstellar Probe mission, in *Proceedings of the Space Technology and Application International Forum 1999*, Am. Inst. of Phys., College Park, Md., in press, 2000.

Luhmann, J.G., Oxygen in the heliosphere, *J. Geophys. Res.*, 99, 13,285-13,305, 1994.

McComas, D.J., et al., Ulysses' return to the slow solar wind, *Geophys. Res. Lett.*, 25, 1-4, 1998.

Meier, R.R., The scattering rate of solar 834 Å radiation by magnetospheric O+ and O++, *Geophys. Res. Lett.*, 17, 1613-1616, 1990.

Meier, R.R., Ultraviolet spectroscopy and remote sensing of the upper atmosphere, *Space Sci. Rev.*, 58, 1-185, 1991.

Moebius, E., The local interstellar medium viewed through pickup ions: recent results and future perspectives, *Space Sci. Rev.*, 78, 375-386, 1996.

Moebius, E., et al., Direct observation of He$^+$ pickup ions of interstellar origin in the solar wind, *Nature, 318*, 426-429, 1985.

Paresce, F., and P. Jakobsen, The diffuse UV background, *Nature, 288*, 119-126, 1980.

Parker, E.N., The stellar-wind regions, *Astrophys. J., 134*, 20-27, 1961.

Reynolds, R.J., A lower limit on the ionization fraction of the very local interstellar medium, in *Physics of the Outer Heliosphere*, edited by S. Grzedzielski and D.E. Page, pp. 101-104, Pergamon, Tarrytown, N.Y., 1990.

Suess, S.T., The heliopause, *Rev. Geophys., 28*, 97-115, 1990.

Thomas, G.E., The interstellar wind and its influence on the interplanetary environment, *Annu. Rev. Earth Planet. Sci., 6*, 173-204, 1978.

Tousey, R., J.D. Purcell, W.E. Austin, D.L. Garrett, and K.G. Widing, New photographic spectra of the sun in the extreme ultraviolet, *Space Res., 4*, 703718, 1963

Vallerga, J., Observations of the local interstellar medium with the Extreme Ultraviolet Explorer, *Space Sci. Rev., 78*, 277-288, 1996.

Vallerga, J., The stellar extreme-ultraviolet radiation field, *Astrophys. J., 497*, 921-927, 1998.

Vallerga, J.V., and B.Y. Welsh, ε Canis Majoris and the ionization of the local cloud, *Astrophys. J., 444*, 702-707, 1995.

Warren, H.P., J.T. Mariska, and J. Lean, A new reference spectrum for the EUV irradiance of the quiet Sun, 1, Emission measure formulation, *J. Geophys. Res., 103*, 12,077-12,089, 1998.

Witte, M., M. Banaszkiewicz, and H. Rosenbauer, Recent results on the parameters of the interstellar helium from the Ulysses/GAS experiment, *Space Sci. Rev., 78*, 289-296, 1996.

Wood, B.E., and J.L. Linsky, The local ISM and its interaction with the winds of nearby late-type stars, *Astrophys. J., 492*, 788-803, 1998.

M. Gruntman, Department of Aerospace Engineering, MC-1191, University of Southern California, Los Angeles, CA 90089-1191. (mikeg@spock.usc.edu)

H. J. Fahr, Institut für Astrophysik und Extraterrestrische Forschung, Universität Bonn, Auf dem Hügel 71, Bonn D-53121, Germany.